

Bit-Slicing the Hilbert Space: Scaling Up Accurate Quantum Circuit Simulation to a New Level

Yuan-Hung Tsai[†], Jie-Hong R. Jiang^{†‡}, and Chiao-Shan Jhang[‡]

[†]Graduate Institute of Electronics Engineering, [‡]Department of Electrical Engineering
National Taiwan University, Taipei, Taiwan

Abstract—Quantum computing is greatly advanced in recent years and is expected to transform the computation paradigm in the near future. Quantum circuit simulation plays a key role in the toolchain for the development of quantum hardware and software systems. However, due to the enormous Hilbert space of quantum states, simulating quantum circuits with classical computers is extremely challenging despite notable efforts have been made. In this paper, we enhance quantum circuit simulation in two dimensions: accuracy and scalability. The former is achieved by using an algebraic representation of complex numbers; the latter is achieved by bit-slicing the number representation and replacing matrix-vector multiplication with symbolic Boolean function manipulation. Experimental results demonstrate that our method can be superior to the state-of-the-art for various quantum circuits and can simulate certain benchmark families with up to tens of thousands of qubits.

I. INTRODUCTION

Recent progress in building quantum computers has set the milestone of demonstrating quantum supremacy [1]. Quantum computation is expected to provide computing power beyond the reach of classical computers and transform the information technology in the near future. Quantum hardware and software systems, e.g., [2], [3], are under active development. Quantum system design requires a comprehensive software toolchain, where quantum circuit simulation is one of the key components.

Simulating quantum circuits on a classical computer is indispensable to understand system behavior and verify design correctness especially before universal quantum computers are ready. However the simulation is challenging because quantum states have to be described in the complex vector space and the space is exponential in the number of quantum bits (qubits). Although there are special classes of quantum circuits, such as the stabilizer circuits, that allow efficient simulation by classical computers, see, e.g., [4], simulating general quantum circuits can be extremely difficult. In fact, it is this difficulty that triggered Richard Feynman envisaging quantum simulators/computers in his seminal lecture on 'Simulating Physics with Computers' in 1981.

Despite the aforementioned challenges, various simulation algorithms have been proposed and tools are available to date. Depending on the underlying data structure, existing methods can be mainly classified into array-based, e.g., [5]–[9], or decision-diagram (DD) based, e.g., [10]–[13]. The former is rather limited without exploiting supercomputing facilities and hardly scalable to 50 qubits even with supercomputing. On the other hand, although decision diagrams are well-known for their typical memory explosion problems, the latter

when engineered properly can be superior to the former [12]. The simulation method proposed in this work is DD-based. While prior DD-based methods [10], [13], [14] require specializing multi-terminal or multi-valued DDs for general quantum circuit simulation, ours relies on standard binary decision diagrams (BDDs) and takes an off-the-shelf BDD package for computation.

The state-of-the-art methods [12], [13] are based on the Quantum Multiple-valued Decision Diagrams (QMDDs) [14]. The data structure consists of decision nodes with multi-valued branching for matrix representation and edges weighted with complex numbers for unitary operator and state vector representation and manipulation. In contrast, we simply rely on BDD to represent quantum states and support matrix and vector multiplication. Moreover, unlike prior work [12], [13] with precision loss representing complex numbers, our method employs the algebraic representation [15] for accurate complex number representation under the considered set of unitary operators (see Table I) general enough to achieve universal quantum computation. Note that although the QMDD-based methods can potentially benefit from algebraic representation, it cannot be done as easy as ours due to the complications of unique representation and division by normalization factors [15]. To the best of our knowledge, our method is the first work that utilizes the accurate representation for quantum circuit simulation.

In addition to the accuracy enhancement, to extend the capacity of quantum circuit simulation, we devise 1) a bit-slicing technique that represents a state vector bit by bit each corresponds to a BDD, and 2) an implicit method that replaces matrix-vector multiplication with a set of precharacterized Boolean formulas of the unitary operators for BDD manipulation. Experimental results demonstrate the accuracy and scalability advantages of the proposed method compared to the state-of-the-art over a number of different benchmarks. Notably for certain benchmark families, our method can simulate circuits up to tens of thousands of qubits beyond the capacity of other existing simulators. While encouraged by the strengths of our approach, we also identify some weaknesses for future improvements.

The rest of the paper is organized as follows. In Section II, preliminaries are given. The main simulation algorithm is then presented in Section III. Section IV shows the experimental results and evaluates different simulation methods. Finally in Section V we concludes this paper and outline some directions for future work.

II. PRELIMINARIES

For convention in the sequel, variables are denoted with lower-case letters, e.g. x , while Boolean functions and their BDD representations are denoted with upper-case letters, e.g., F . We denote Boolean connectives negation by overline or \neg , conjunction by \wedge , disjunction by \vee , and exclusive-or by \oplus . We sometimes omit \wedge in a Boolean formula.

A *literal* is a Boolean variable, e.g., x , in the positive phase, or its negation, e.g., $\neg x$, in the negative phase. Let $var(\ell)$ denote the underlying variable of literal ℓ ; let $phase(\ell)$ denote the phase of ℓ for $phase(\ell) = 1$ if $\ell = \delta(\ell)$ and $phase(\ell) = 0$ otherwise. A *cube* is a conjunction of literals, which is treated as a set of literals.

The *cofactor* of a Boolean function (BDD) F with respect to a literal ℓ is denoted by $F|_{\ell}$, which corresponds to the new Boolean function same as F expect for variable $var(\ell)$ in F being substituted with $phase(\ell)$. The notion of cofactor is straightforwardly generalized to a cube q so that F is cofactored with respect to the literals in q .

A. Quantum Circuit Basics

Quantum computation through quantum circuit execution takes three actions: 1) initial state preparation, 2) state evolution via quantum circuit operation, 3) qubit measurement. A quantum circuit simulator has to implement algorithms to perform these actions as detailed in the following.

1) *Initial State Preparation*: Unlike a classical bit takes value either 0 (in other words, in state 0, denoted $|0\rangle$) or 1 (in state 1, denoted $|1\rangle$), a qubit in state $|\psi\rangle$ can be in a superposition state of both $|0\rangle$ and $|1\rangle$ described by

$$|\psi\rangle = \alpha \cdot |0\rangle + \beta \cdot |1\rangle$$

where $\alpha, \beta \in \mathbb{C}$ are *probability amplitudes* satisfying the normalization constraint $|\alpha|^2 + |\beta|^2 = 1$. For an n -qubit quantum system, the qubits can be entangled and an n -qubit state $|\psi\rangle$ can be described by

$$|\psi\rangle = \sum_{i \in \{0,1\}^n} \alpha_i \cdot |i\rangle, \quad (1)$$

where the probability amplitudes $\alpha_i \in \mathbb{C}$ satisfy


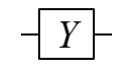
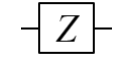
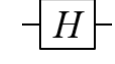
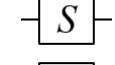
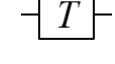
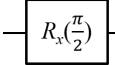
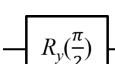
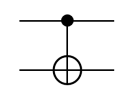
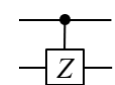
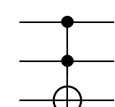
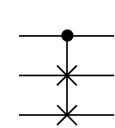
$$\sum_{i \in \{0,1\}^n} |\alpha_i|^2 = 1. \quad (2)$$

Therefore, a quantum state of n qubits can be alternatively represented as a 2^n -dimensional state vector $[\alpha_0, \dots, \alpha_{2^n-1}]^T$.

For initial state preparation, a quantum circuit simulator needs to construct a state vector representing some specified initial quantum state.

2) *State Evolution via Quantum Circuit Operation*: The state of a quantum system can be updated by the application of quantum operations (or so-called quantum gates). The functionality of a quantum operation applied on n qubits can be described by a $2^n \times 2^n$ dimensional *unitary matrix* U (satisfying $U^{-1} = U^\dagger$, that is, its inverse matrix equals its Hermitian adjoint). The quantum gates considered in this work are listed in Table I.

TABLE I
QUANTUM GATES SUPPORTED IN THIS WORK.

Gate	Symbol	Matrix
Pauli-X (X)		$\begin{bmatrix} 0 & 1 \\ 1 & 0 \end{bmatrix}$
Pauli-Y (Y)		$\begin{bmatrix} 0 & -i \\ i & 0 \end{bmatrix}$
Pauli-Z (Z)		$\begin{bmatrix} 1 & 0 \\ 0 & -1 \end{bmatrix}$
Hadamard (H)		$\frac{1}{\sqrt{2}} \begin{bmatrix} 1 & 1 \\ 1 & -1 \end{bmatrix}$
Phase (S)		$\begin{bmatrix} 1 & 0 \\ 0 & i \end{bmatrix}$
T		$\begin{bmatrix} 1 & 0 \\ 0 & e^{i\pi/4} \end{bmatrix}$
Rx($\frac{\pi}{2}$)		$\frac{1}{\sqrt{2}} \begin{bmatrix} 1 & -i \\ -i & 1 \end{bmatrix}$
Ry($\frac{\pi}{2}$)		$\frac{1}{\sqrt{2}} \begin{bmatrix} 1 & -1 \\ 1 & 1 \end{bmatrix}$
Controlled-NOT (CNOT)		$\begin{bmatrix} 1 & 0 & 0 & 0 \\ 0 & 1 & 0 & 0 \\ 0 & 0 & 0 & 1 \\ 0 & 0 & 1 & 0 \end{bmatrix}$
Controlled-Z (CZ)		$\begin{bmatrix} 1 & 0 & 0 & 0 \\ 0 & 1 & 0 & 0 \\ 0 & 0 & 1 & 0 \\ 0 & 0 & 0 & -1 \end{bmatrix}$
Toffoli		$\begin{bmatrix} 1 & 0 & 0 & 0 & 0 & 0 & 0 & 0 \\ 0 & 1 & 0 & 0 & 0 & 0 & 0 & 0 \\ 0 & 0 & 1 & 0 & 0 & 0 & 0 & 0 \\ 0 & 0 & 0 & 1 & 0 & 0 & 0 & 0 \\ 0 & 0 & 0 & 0 & 1 & 0 & 0 & 0 \\ 0 & 0 & 0 & 0 & 0 & 1 & 0 & 0 \\ 0 & 0 & 0 & 0 & 0 & 0 & 1 & 0 \\ 0 & 0 & 0 & 0 & 0 & 0 & 0 & 1 \end{bmatrix}$
Fredkin		$\begin{bmatrix} 1 & 0 & 0 & 0 & 0 & 0 & 0 & 0 \\ 0 & 1 & 0 & 0 & 0 & 0 & 0 & 0 \\ 0 & 0 & 1 & 0 & 0 & 0 & 0 & 0 \\ 0 & 0 & 0 & 1 & 0 & 0 & 0 & 0 \\ 0 & 0 & 0 & 0 & 1 & 0 & 0 & 0 \\ 0 & 0 & 0 & 0 & 0 & 1 & 0 & 0 \\ 0 & 0 & 0 & 0 & 0 & 0 & 1 & 0 \\ 0 & 0 & 0 & 0 & 0 & 0 & 0 & 1 \end{bmatrix}$

Consequently the state of a quantum system can be updated by multiplying a state vector with a unitary matrix. For a quantum circuit with m gates corresponding to unitary operators M_1, \dots, M_m in order, let v_0 be the initial input state and v_m be the final output state of the circuit. Then

$$v_m = M_m \times M_{m-1} \times \dots \times M_1 \times v_0. \quad (3)$$

3) *Qubit Measurement*: After all quantum gates are applied, we may need to measure some qubits to get their state outcome and determine its probability. In quantum mechanics, measuring a qubit makes its state collapse (with superposition being destroyed) into an eigenstate with respect to the measurement basis. The probability of an eigenstate being observed is determined by its corresponding probability amplitude. Specifically, the probability of qubit q being collapsed to $|0\rangle$ (similarly $|1\rangle$) can be calculated by

$$\Pr[q = |0\rangle] = \sum_{i \in \{0,1\}^n \text{ with bit } q=0} |\alpha_i|^2. \quad (4)$$

Suppose after measuring qubit q , it collapses to state $|0\rangle$, say. Then the quantum state of the n -qubit system will have 0 probability amplitudes for states $|i\rangle$ for $i \in \{0, 1\}^n$ with bit q being 1. Consequently the probability amplitudes for the other states, i.e., $|i\rangle$ for $i \in \{0, 1\}^n$ with bit q being 0, are renormalized by the factor $1/\sqrt{\Pr[q = |0\rangle]}$.

Note that the measurement process can be repeated for some other qubits sequentially or simultaneously.

III. BDD-BASED QUANTUM SIMULATION

In this section, we describe the proposed BDD-based structure for representing state vectors, and provide methods to complete quantum simulation on this BDD-based structure, i.e., realize three actions discussed in Section II.

A. Algebraic Representation of Complex Values

In this work, we employ the algebraic representation of complex values proposed in [15] to achieve *accurate* quantum simulation without precision loss. Essentially, any complex value (scalar) α that can be represented exactly can be expressed as

$$\alpha = \frac{1}{\sqrt{2^k}}(a\omega^3 + b\omega^2 + c\omega + d), \quad (5)$$

where the coefficients $a, b, c, d, k \in \mathbb{Z}$, $\alpha \in \mathbb{C}$, and $\omega = e^{i\pi/4}$. Therefore, in the context of quantum circuit simulation, when all the entries in the initial state vector and the unitary operators can be exactly represented, all the complex values result from the matrix-vector multiplication can be exactly represented, too.

The representation is appealing as we only need to maintain five integers to represent a complex number. By a simple counting argument that \mathbb{Z}^5 is countable while \mathbb{C} is uncountable, clearly not every complex number can be compactly represented in this algebraic form. However as there are universal gate sets, such as the Clifford+T set, for quantum computing whose entries are all exactly representable, quantum circuit simulation under the algebraic representation can be generally done without loss of generality. It is because the universality of a gate set allows any unitary operator to be approximated using the gates from the set within any desired precision. Hence as long as the initial state can be exactly represented, quantum circuit simulation can be achieved without precision loss.

The next question we should address is how to efficiently maintain and manipulate the integers for quantum circuit simulation.

B. Bit-Slicing State Vectors with BDDs

Given a state vector $|\psi\rangle$ of an n -qubit quantum system with its entries represented algebraically in the form of Eq. (5), we exploit BDDs for representation as follows.

By Eq. (5), the state vector $|\psi\rangle$ (with 2^n entries of complex values) is described by an integer scalar k and four vectors $\vec{a} = [a_0, \dots, a_{2^n-1}]^T$, $\vec{b} = [b_0, \dots, b_{2^n-1}]^T$, $\vec{c} = [c_0, \dots, c_{2^n-1}]^T$, $\vec{d} = [d_0, \dots, d_{2^n-1}]^T$, each with 2^n entries of integer values. Hence the probability amplitude α_i of basis state $|i\rangle$ in $|\psi\rangle$ equals $\frac{1}{\sqrt{2^k}}(a_i\omega^3 + b_i\omega^2 + c_i\omega + d_i)$ for

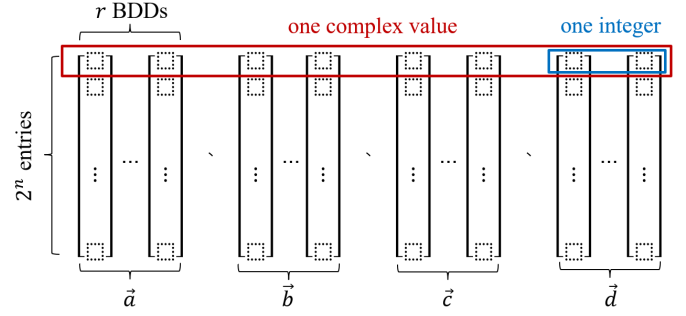


Fig. 1. Bit-slicing algebraic numbers with BDDs.

$i \in \{0, 1\}^n$. Let a_i, b_i, c_i, d_i be r -bit integers (r can be adjusted on-the-fly as large as enough in our implementation). We represent the j^{th} bit, for $j = 1, \dots, r$, of each of the vectors $\vec{a}, \vec{b}, \vec{c}, \vec{d}$ with a BDD as illustrated in Fig. 1. Thereby each BDD is a function over the n qubit variables so that the truth table of the function corresponds to the corresponding a bit vector of 2^n entries. On the other hand, because scalar k is shared among all 2^n entries of $\vec{a}, \vec{b}, \vec{c}, \vec{d}$, it is stored separately. Overall we use $4r$ BDDs over n variables to represent an n -qubit state vector. In the sequel, we denote the BDDs of the i^{th} bit of $\vec{a}, \vec{b}, \vec{c}$, and \vec{d} as F^{ai}, F^{bi}, F^{ci} , and F^{di} , respectively.

Note that we require no algebraic representation for unitary matrices as we replace matrix-vector multiplication with Boolean formula manipulation over state-vector BDDs as to be explained in Section III-D.

C. Initial State Construction

A typical, if not every, quantum computation algorithm prepares its initial state in one of the basis states specified *a priori*. In this case, all BDDs correspond to constant 0 (logical false) except for F^{d0} . Given an n -qubit quantum circuit with an initial state $|i\rangle = |b_0 \dots b_{n-1}\rangle$ for some $i \in \{0, 1\}^n$ and $b_0, \dots, b_{n-1} \in \{0, 1\}$, then

$$F^{d0} = \bigwedge_{j=0}^{n-1} l_j, \quad \text{for } l_j = \begin{cases} \bar{q}_j, & \text{if } b_j = 0 \\ q_j, & \text{if } b_j = 1 \end{cases}, \quad (6)$$

where q_j is the Boolean variable of the formula/BDD under construction corresponding to the j^{th} qubit of the quantum circuit.

D. Unitary State Evolution via Formula Manipulation

Under the bit-sliced state vector representation using BDDs as detailed in Section III-B, we show how to update a state vector when an quantum gate in Table I is applied. Essentially, the new state is the result of the matrix-vector multiplication.

We note that the gates in Table I form a library general enough to achieve universal quantum computation as it is a superset of the Clifford+T [16] as well as the Toffoli+Hadamard [17] universal gate sets.

To avoid vector-matrix multiplication but achieve the same computation, we examine the effect of every considered quantum gate and characterize its corresponding Boolean formulas for updating the bit-sliced algebraic parameters $(\vec{a}, \vec{b}, \vec{c}, \vec{d}, k)$ stated in Section III-B. The obtained update rules

for F^{ai} , F^{bi} , F^{ci} , F^{di} are summarized in Table II. For brevity, below we only detail the update rule derivation of H-gate while leaving others as exercises for interested readers to verify.

For simplicity, consider a 2-qubit quantum system with the state vector $[\alpha_0, \alpha_1, \alpha_2, \alpha_3]^T$, where α_0 , α_1 , α_2 , and α_3 are the probability amplitudes of basis states $|q_0q_1\rangle = |00\rangle$, $|01\rangle$, $|10\rangle$, and $|11\rangle$, respectively. Without loss of generality, assume a Hadamard gate is applied on qubit q_0 . The unitary matrix for the 2-qubit system is then obtained by the Kronecker product

$$H \otimes I = \frac{1}{\sqrt{2}} \begin{bmatrix} 1 & 1 \\ 1 & -1 \end{bmatrix} \otimes \begin{bmatrix} 1 & 0 \\ 0 & 1 \end{bmatrix} = \frac{1}{\sqrt{2}} \begin{bmatrix} 1 & 0 & 1 & 0 \\ 0 & 1 & 0 & 1 \\ 1 & 0 & -1 & 0 \\ 0 & 1 & 0 & -1 \end{bmatrix}.$$

With the scaling factor $\frac{1}{\sqrt{2}}$ being omitted (which contributes to the increment of parameter k by 1), the state vector is updated to

$$\begin{bmatrix} 1 & 0 & 1 & 0 \\ 0 & 1 & 0 & 1 \\ 1 & 0 & -1 & 0 \\ 0 & 1 & 0 & -1 \end{bmatrix} \begin{bmatrix} \alpha_0 \\ \alpha_1 \\ \alpha_2 \\ \alpha_3 \end{bmatrix} = \begin{bmatrix} \alpha_0 + \alpha_2 \\ \alpha_1 + \alpha_3 \\ \alpha_0 - \alpha_2 \\ \alpha_1 - \alpha_3 \end{bmatrix} = \begin{bmatrix} \alpha_0 \\ \alpha_1 \\ \alpha_0 \\ \alpha_1 \end{bmatrix} + \begin{bmatrix} \alpha_2 \\ \alpha_3 \\ -\alpha_2 \\ -\alpha_3 \end{bmatrix}.$$

The summation of the above two vectors forms the basis of updating F^{ai} , F^{bi} , F^{ci} , F^{di} for the Hadamard gate.

For a general n -qubit quantum system, the following proposition specifies the formulas that update F^{ai} (similarly F^{bi} , F^{ci} , F^{di}) of the original state vector to \hat{F}^{ai} of the new state vector.

Proposition 1. For an n -qubit quantum system with its state vector being algebraically represented with F^{ai} (along with F^{bi} , F^{ci} , F^{di}), let Hadamard gate be applied on an arbitrary qubit q_t . Then the new state vector is specified by \hat{F}^{ai} (along with \hat{F}^{bi} , \hat{F}^{ci} , \hat{F}^{di} derivable similarly) as follows.

$$G^{ai} = F^{ai}|_{\bar{q}_t}, \quad (7)$$

$$D^{ai} = \bar{q}_t F^{ai}|_{q_t} \vee q_t \overline{F^{ai}}, \quad (8)$$

$$C^{a0} = q_t, \quad (9)$$

$$C^{a(i+1)} = G^{ai} D^{ai} \vee (G^{ai} \vee D^{ai}) C^{ai}, \quad (10)$$

$$\hat{F}^{ai} = G^{ai} \oplus D^{ai} \oplus C^{ai}, \quad (11)$$

where $i = 0, \dots, r-1$ for r be the integer size of algebraic parameters $(\vec{a}, \vec{b}, \vec{c}, \vec{d})$. Moreover, the k -value increases by 1.

To see the correctness (with the help of the above 2-qubit example), observe that Eq. (7) and Eq. (8) derive the BDDs of two component vectors ($[\alpha_0, \alpha_1, \alpha_0, \alpha_1]^T$ and $[\alpha_2, \alpha_3, -\alpha_2, -\alpha_3]^T$, respectively). Moreover, Eq. (9), Eq. (10) and Eq. (11) together fulfill the function of an adder summing the two component vectors bitwisely. It is worth noting that since we use 2's complement to represent integers, we set $C^{a0} = q_t$ in Eq. (9) as the initial carry-in of the adder function to realize the "plus one" action for the negated entries of the second component vector (in $[\alpha_2, \alpha_3, -\alpha_2, -\alpha_3]^T$ the last two entries are complemented in Eq. (8) by the second term, i.e., $q_t \overline{F^{ai}}$, and their "plus one" actions are realized by the initial carry-in setting). On the other hand, the Hadamard gate increases the k -value by 1 due to the $\frac{1}{\sqrt{2}}$ scaling factor.

For other quantum gates, their F^{ai} , F^{bi} , F^{ci} , and F^{di} formulas are obtained and summarized in Table II, where q_c is the control bit, Q_c is the conjunction of all control bits of the Toffoli and Fredkin gate, q_t is the target bit, $q_{t'}$ is the second target for Fredkin gates, and $i = 0, \dots, r-1$. Also in the table, for brevity we define

$$\text{Car}(A, B, C) \triangleq AB \vee (A \vee B)C,$$

$$\text{Sum}(A, B, C) \triangleq A \oplus B \oplus C,$$

to denote the *carry* and *sum* operations over formulas A, B, C . We note that the formulas of the Toffoli gate in the table work for a general Toffoli gate of an arbitrary number of control bits. Note also that quantum gates X, Z, H, $\text{Ry}(\frac{\pi}{2})$, CNOT, CZ, Toffoli, and Fredkin involve no imaginary parts and thus their F^{ai} , F^{bi} , F^{ci} , and F^{di} formulas are mutually independent. In contrast, quantum gates Y, S, T, and $\text{Rx}(\frac{\pi}{2})$ involve imaginary parts and cause phase shifts making their F^{ai} , F^{bi} , F^{ci} , and F^{di} formulas mutually dependent. About the algebraic parameter k , its value remains the same for all the quantum gates except for being incremented by 1 for Hadamard, $\text{Rx}(\pi/2)$, and $\text{Ry}(\pi/2)$ gates due to their $\frac{1}{\sqrt{2}}$ scaling factors.

The correctness of Table II construction is asserted in the following theorem.

Theorem 1. The formulas F^{ai} , F^{bi} , F^{ci} , F^{di} of Table II and the k value update rule stated above correctly update the quantum state under the algebraic representation of Eq. (5).

We mention that in our implementation the integer bit size r is augmented dynamically when necessary (i.e., overflow occurs). Thereby with the accuracy guarantee of the algebraic representation, our simulation is exact (i.e., no precision loss).

E. Measurement and Probability Calculation

In the QMDD-based method [12], measurement and probability calculation can be done efficiently by traversing the QMDD. For a qubit q to be measured, placing it as the top variable of the QMDD makes $\text{Pr}[q = |0\rangle]$ and $\text{Pr}[q = |1\rangle]$ derivable in one QMDD traversal.

In our case, measurement and probability calculation are not as easy as the QMDD case because we do not have a monolithic BDD but rather $4r$ BDDs. We adopt the hyperfunction construction [18] of combining multiple BDDs into one monolithic BDD F as follows. Let

$$F = x_0 x_1 F^{\vec{a}} \vee x_0 \bar{x}_1 F^{\vec{b}} \vee \bar{x}_0 x_1 F^{\vec{c}} \vee \bar{x}_0 \bar{x}_1 F^{\vec{d}}, \quad (12)$$

for

$$F^{\vec{a}} = \bigvee_{i=0}^{r-1} g_i F^{ai}, F^{\vec{b}} = \bigvee_{i=0}^{r-1} g_i F^{bi},$$

$$F^{\vec{c}} = \bigvee_{i=0}^{r-1} g_i F^{ci}, F^{\vec{d}} = \bigvee_{i=0}^{r-1} g_i F^{di},$$

TABLE II
 BOOLEAN FORMULAS FOR QUANTUM STATE EVOLUTION OF THE SUPPORTED GATE SET.

Gate	Update F^{ai}	Update F^{bi}	Boolean formulas	Update F^{ci}	Update F^{di}
X	$\hat{F}^{ai} = q_t F^{ai} _{\bar{q}_t} \vee \bar{q}_t F^{ai} _{q_t}$.			same as F^{ai} except renaming	
Y	$G^{ai} = q_t F^{ci} _{\bar{q}_t} \vee \bar{q}_t F^{ci} _{q_t}$, $D^{ai} = q_t G^{ai} \vee \bar{q}_t \bar{G}^{ai}$, $C^{a0} = \bar{q}_t$, $C^{a(i+1)} = \text{Car}(D^{ai}, 0, C^{ai})$, $\hat{F}^{ai} = \text{Sum}(D^{ai}, 0, C^{ai})$.	$G^{bi} = q_t F^{di} _{\bar{q}_t} \vee \bar{q}_t F^{di} _{q_t}$, $D^{bi} = q_t G^{bi} \vee \bar{q}_t \bar{G}^{bi}$, $C^{b0} = \bar{q}_t$, $C^{b(i+1)} = \text{Car}(D^{bi}, 0, C^{bi})$, $\hat{F}^{bi} = \text{Sum}(D^{bi}, 0, C^{bi})$.	$G^{ci} = q_t F^{ai} _{\bar{q}_t} \vee \bar{q}_t F^{ai} _{q_t}$, $D^{ci} = q_t \bar{G}^{ci} \vee \bar{q}_t G^{ci}$, $C^{c0} = q_t$, $C^{c(i+1)} = \text{Car}(D^{ci}, 0, C^{ci})$, $\hat{F}^{ci} = \text{Sum}(D^{ci}, 0, C^{ci})$.	$G^{di} = q_t F^{bi} _{\bar{q}_t} \vee \bar{q}_t F^{bi} _{q_t}$, $D^{di} = q_t \bar{G}^{di} \vee \bar{q}_t G^{di}$, $C^{d0} = q_t$, $C^{d(i+1)} = \text{Car}(D^{di}, 0, C^{di})$, $\hat{F}^{di} = \text{Sum}(D^{di}, 0, C^{di})$.	
Z	$G^{ai} = \bar{q}_t F^{ai} \vee q_t \bar{F}^{ai}$, $C^{a0} = q_t$, $C^{a(i+1)} = \text{Car}(G^{ai}, 0, C^{ai})$, $\hat{F}^{ai} = \text{Sum}(G^{ai}, 0, C^{ai})$.			same as F^{ai} except renaming	
H	$G^{ai} = F^{ai} _{\bar{q}_t}$, $D^{ai} = \bar{q}_t F^{ai} _{q_t} \vee q_t \bar{F}^{ai}$, $C^{a0} = q_t$, $C^{a(i+1)} = \text{Car}(G^{ai}, D^{ai}, C^{ai})$, $\hat{F}^{ai} = \text{Sum}(G^{ai}, D^{ai}, C^{ai})$.			same as F^{ai} except renaming	
S	$\hat{F}^{ai} = \bar{q}_t F^{ai} \vee q_t F^{ci}$.	$\hat{F}^{bi} = \bar{q}_t F^{bi} \vee q_t F^{di}$.		$G^{ci} = \bar{q}_t F^{ci} \vee q_t \bar{F}^{ai}$, $C^{c0} = q_t$, $C^{c(i+1)} = \text{Car}(G^{ci}, 0, C^{ci})$, $\hat{F}^{ci} = \text{Sum}(G^{ci}, 0, C^{ci})$.	$G^{di} = \bar{q}_t F^{di} \vee q_t \bar{F}^{bi}$, $C^{d0} = q_t$, $C^{d(i+1)} = \text{Car}(G^{di}, 0, C^{di})$, $\hat{F}^{di} = \text{Sum}(G^{di}, 0, C^{di})$.
T	$\hat{F}^{ai} = \bar{q}_t F^{ai} \vee q_t F^{bi}$.	$\hat{F}^{bi} = \bar{q}_t F^{bi} \vee q_t F^{ci}$.		$\hat{F}^{ci} = \bar{q}_t F^{ci} \vee q_t F^{di}$.	$G^{di} = \bar{q}_t F^{di} \vee q_t \bar{F}^{ai}$, $C^{d0} = q_t$, $C^{d(i+1)} = \text{Car}(G^{di}, 0, C^{di})$, $\hat{F}^{di} = \text{Sum}(G^{di}, 0, C^{di})$.
Rx($\frac{\pi}{2}$)	$D^{ai} = q_t F^{ci} _{\bar{q}_t} \vee \bar{q}_t F^{ci} _{q_t}$, $C^{a0} = 1$, $C^{a(i+1)} = \text{Car}(F^{ai}, \bar{D}^{ai}, C^{ai})$, $\hat{F}^{ai} = \text{Sum}(F^{ai}, \bar{D}^{ai}, C^{ai})$.	$D^{bi} = q_t F^{di} _{\bar{q}_t} \vee \bar{q}_t F^{di} _{q_t}$, $C^{b0} = 1$, $C^{b(i+1)} = \text{Car}(F^{bi}, \bar{D}^{bi}, C^{bi})$, $\hat{F}^{bi} = \text{Sum}(F^{bi}, \bar{D}^{bi}, C^{bi})$.	$D^{ci} = q_t F^{ai} _{\bar{q}_t} \vee \bar{q}_t F^{ai} _{q_t}$, $C^{c0} = 0$, $C^{c(i+1)} = \text{Car}(F^{ci}, D^{ci}, C^{ci})$, $\hat{F}^{ci} = \text{Sum}(F^{ci}, D^{ci}, C^{ci})$.	$D^{di} = q_t F^{bi} _{\bar{q}_t} \vee \bar{q}_t F^{bi} _{q_t}$, $C^{d0} = 0$, $C^{d(i+1)} = \text{Car}(F^{di}, D^{di}, C^{di})$, $\hat{F}^{di} = \text{Sum}(F^{di}, D^{di}, C^{di})$.	
Ry($\frac{\pi}{2}$)	$G^{ai} = F^{ai} _{\bar{q}_t}$, $D^{ai} = q_t F^{ai} \vee \bar{q}_t \bar{F}^{ai} _{q_t}$, $C^{a0} = \bar{q}_t$, $C^{a(i+1)} = \text{Car}(G^{ai}, D^{ai}, C^{ai})$, $\hat{F}^{ai} = \text{Sum}(G^{ai}, D^{ai}, C^{ai})$.			same as F^{ai} except renaming	
CNOT	$\hat{F}^{ai} = \bar{q}_c F^{ai} \vee q_c q_t F^{ai} _{q_c \bar{q}_t} \vee q_c \bar{q}_t F^{ai} _{q_c q_t}$.			same as F^{ai} except renaming	
CZ	$G^{ai} = \bar{q}_c \bar{q}_t F^{ai} \vee q_c q_t \bar{F}^{ai}$, $C^{a0} = q_c q_t$, $C^{a(i+1)} = \text{Car}(G^{ai}, 0, C^{ai})$, $\hat{F}^{ai} = \text{Sum}(G^{ai}, 0, C^{ai})$.			same as F^{ai} except renaming	
Toffoli	$\hat{F}^{ai} = \bar{Q}_c F^{ai} \vee Q_c q_t F^{ai} _{Q_c \bar{q}_t} \vee Q_c \bar{q}_t F^{ai} _{Q_c q_t}$.			same as F^{ai} except renaming	
Fredkin	$\hat{F}^{ai} = \bar{Q}_c (q_t \oplus q_{t'}) F^{ai} \vee Q_c q_t q_{t'} F^{ai} _{Q_c \bar{q}_t q_{t'}} \vee Q_c \bar{q}_t q_{t'} F^{ai} _{Q_c q_t \bar{q}_{t'}}$.			same as F^{ai} except renaming	

with

$$g_i = \begin{cases} \overline{x_2 x_3 \cdots x_{\lceil \log_2 r \rceil + 1}}, & \text{if } i = 0 \\ x_2 \overline{x_3 \cdots x_{\lceil \log_2 r \rceil + 1}}, & \text{if } i = 1 \\ \overline{x_2 x_3 \cdots x_{\lceil \log_2 r \rceil + 1}}, & \text{if } i = 2 \\ \vdots & \\ x_2 x_3 \cdots x_{\lceil \log_2 r \rceil + 1}, & \text{if } i = r - 1 \end{cases},$$

where x_0 to $x_{\lceil \log_2 r \rceil + 1}$ are fresh new Boolean variables used for labeling/encoding the $4r$ BDDs.

Given a monolithic BDD F , the measurement procedure is conducted on F as illustrated in Fig. 2, where the qubit variables q_0, \dots, q_{n-1} are ordered above the encoding variables x_0, x_1 , which are followed by variables $x_2 \dots, x_{\lceil \log_2 r \rceil + 1}$ variables, and p_{ij} denotes the probability $\Pr[q_i = |j\rangle]$ for $j \in \{0, 1\}$. For probability calculation of measurement, we compute the accumulated probabilities of the nodes at the top n levels recursively, and record them by a hash map. (The accumulated probability of a node is the sum of the probabilities of its left and right children.) If the recursive procedure reaches the n^{th} level of F (counting from 0), the four algebraic integers a, b, c , and d can be decoded by paths $x_0 x_1, x_0 \overline{x_1}, \overline{x_0} x_1$, and $\overline{x_0} \overline{x_1}$, respectively, to obtain values of the bit positions, and the corresponding probability amplitude α can be computed.

As mentioned in Section II-A, all probability amplitudes should be multiplied with a normalization factor after some probability amplitudes are set to zero due to measurement. Unfortunately, a normalization factor may not be algebraically represented by Eq. (5). Hence, we modify Eq. (5) as

$$s \times \alpha = s \times \frac{1}{\sqrt{2^k}} (a\omega^3 + b\omega^2 + c\omega + d), \quad (13)$$

where $s \in \mathbb{R}$ is a normalization factor for measuring some qubit(s). Note that the potential precision loss in this final simulation step of measurement is inevitable because we have to represent the answer probability using a floating point number anyway. On the other hand, for measuring multiple qubits, having one measurement on all of the interested qubits yields less precision loss than a sequence of measurements on the qubits one at a time. The former avoids the need of normalization (at the cost of exploring exponential number of outcomes), while the latter requires normalization several times. If our interested query is about the probability of a particular outcome, e.g., $\Pr[q_0 q_1 q_2 = |000\rangle]$, rather than the probabilities of all possible outcomes, then the former is more preferred than the latter.

By replacing α with $s \times \alpha$ in Eq. (4), we derive

$$\sum_{i \in \{0,1\}^n \text{ with } q=j} |s\alpha_i|^2 = s^2 \sum_{i \in \{0,1\}^n \text{ with } q=j} |\alpha_i|^2,$$

where $j \in \{0, 1\}$. Therefore, to compute the current probabilities after normalization, we can simply multiply s^2 with the accumulated probabilities of the current nodes. Hence the accumulated probabilities need not be recomputed due to normalization.

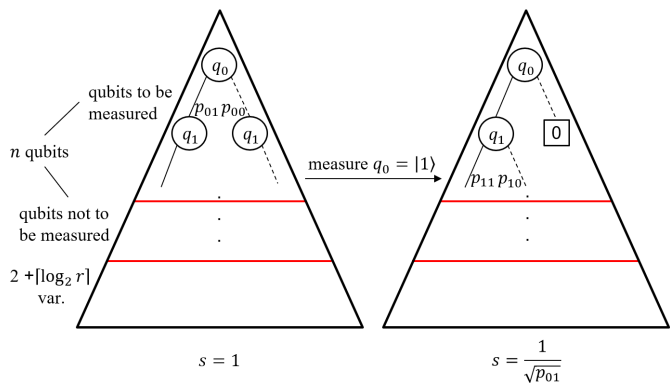


Fig. 2. Monolithic BDD F for measurement.

Assume we would like to measure multiple qubits one at a time. We make the BDD variables of the interested qubits on top and follow the measurement order in F . Without loss of generality let the order be q_0, \dots, q_{n-1} . Then, the first qubit to be measured is q_0 , which is the root node of F . As shown in the left part of Fig. 2, p_{00} and p_{01} are the accumulated probabilities of the 0-child and 1-child of the root node, respectively. Assume we obtain $q_0 = |1\rangle$ after measurement, as shown in the right part of Fig. 2, the amplitudes with $q_0 = |0\rangle$ can easily be set to zero by connecting the 0-edge of q_0 to the constant-0 node, and s is updated from 1 to $1/\sqrt{p_{01}}$ to satisfy the normalization constraint. We repeat the same procedure to measure the other qubits following the order of variables. In fact, when measuring q_i , there exists only one node labelled q_i .

It is worth noting that, when some qubits are to be measured, the order of measuring them is immaterial. This freedom allows BDD reordering to be performed to reduce BDD size. The only requirement is to make the qubit variables to be measured above the qubit variables not to be measured, and the encoding variables below all the qubit variables.

IV. EXPERIMENTAL RESULTS

The proposed simulation algorithm was implemented in C++ in the ABC system [19] and used CUDD [20] as the underlying BDD package. For the dynamic variable reordering heuristic, the implementation of [21] in CUDD was used. In our implementation, the size of the integers r was initially set to 32. When overflows were detected, extra BDDs were allocated for each integer. To reduce the precision loss due to probability calculation in measurement, we used the GNU MPFR library [22] to increase the precision of the floating point numbers. In the experiments, the state-of-the-art simulator DDSIM (version v1.0.1a) [12], [13], which is based on QMDD [14], was compared. All experiments were conducted on a server with Intel(R) Xeon(R) Silver 4210 CPU @ 2.20GHz, 30.7GB RAM. The time-out (TO) limit was set to 7200 seconds, and the memory-out (MO) limit was set to 2GB for each case. The evaluation was performed on four sets of benchmarks, including 1) randomly generated benchmarks, 2) RevLib benchmarks [23] and its variants with entanglements, 3) quantum algorithm benchmarks for

entanglement (Bell state preparation) and BernsteinVazirani (BV) algorithm [24], and 4) supremacy benchmarks from Google [25].

For the first set of benchmarks, we randomly generated circuits of various qubit sizes (40, 80, 120, 160, 200, 300, 400, 500) using all the supported gates, but excluding $R_x(\pi/2)$ and $R_y(\pi/2)$ as they exhibit similar effects as the H-gate. The ratio of $\#gates : \#qubits$ was fixed to 3:1, and 10 circuits were generated for each size. In building a circuit, we first inserted an H-gate to every qubit (so to impose state superposition in the beginning), and then inserted the targeted number of gates into the circuit by picking every gate uniformly at random from the mentioned gate set and applied it to some qubit(s) selected uniformly at random.

The results on the random circuits are shown in Table III, where Column 1 lists $\#qubits$, Column 2 lists $\#gates$, and Columns 3 and 4 list the average runtime and the numbers of TO/MO/error/segmentation fault cases of DDSIM, respectively, and Columns 5 and 6 list the similar information of our simulator. The term ‘error’ indicates a numerical error happened if all state probabilities do not sum to 1 due to precision loss. The message ‘failed’ means all 10 cases cannot be simulated successfully. The reported runtime was only averaged over success cases.

From Table III, we see that DDSIM fails to simulate circuits with 120 or more qubits due to TO, MO, numerical errors, or segmentation faults. In contrast, our method tends to be much more robust and scalable when simulating the considered random circuits. DDSIM yielded 13 MO and 30 error cases. On the contrary, our method produced no such cases. In this benchmark setting, our simulator is superior to DDSIM in runtime, memory efficiency, and accuracy.

For the second benchmark set, we took reversible circuits RevLib [23] for experiments. However, because most of the circuits from RevLib are converted from classical circuits, they do not exhibit quantum effects and can be simulated efficiently. (In the simulation we assumed random initial values for inputs whose initial values are not specified.) To make the circuits more interesting with quantum effects, we modified the original circuits by inserting H-gates to the inputs whose initial values are not specified in the original circuit such that we create superposition states in the beginning. The results on the RevLib benchmarks are shown in Table IV, where Column 1 lists the circuit name, Column 2 lists the corresponding $\#qubits$, Columns 3-5 list the $\#gates$ before the modification and the results on the original circuits, and similarly, Columns 6-8 list the $\#gates$ after the modification and the results on the modified circuits. As one can see from Table IV, both DDSIM and our method can simulate the circuits of classical functionalities efficiently. When the modified circuits are considered, DDSIM suffered mostly from MO when simulating the modified circuits. For those circuits that DDSIM cannot simulate successfully, our method can simulate them within the timeout limit.¹ To further investigate the MO cases of DDSIM, we performed a case study on

¹There are some RevLib benchmarks that our method cannot simulate successfully due to timeout. However, DDSIM fails on those circuits, too.

callif_32_439 and removed the MO limit. Nevertheless, DDSIM still cannot finish simulation within TO limit, and the memory usage grows to 9.72GB upon TO.

For the third benchmark set, we collected quantum algorithm circuits, including the entanglement and BV circuits.² The results are shown in Table V, where Column 1 lists $\#qubits$, Columns 2-4 and 5-7 list the $\#gates$ and runtime information for entanglement and BV circuits, respectively. For the entanglement circuits, DDSIM encountered MO at $\#qubits = 10000$, whereas our method finishes within 67 seconds. For the BV circuits, DDSIM encountered numerical errors and segmentation faults for the $\#qubits \geq 90$ cases, whereas our method finishes in hundreds of seconds when simulating circuits with thousands of qubits. We note that the entanglement circuits belong to the category of stabilizer circuits, which are known efficiently simulatable by classical computers [4]. When CHP [26], a simulator based on [4] dedicated to stabilizer circuit simulation, is applied, the entanglement circuit with $\#qubits = 10000$ can be simulated in 6.7 seconds. It is not surprising as CHP exploits additional circuit properties for fast simulation. On the other hand, BV circuits are beyond the stabilizer circuit category and cannot be simulated by CHP.

For the fourth benchmark set, we took the random circuits proposed by Google for showing quantum supremacy [25].³ These circuits are meant to create highly entangled states to make them challenging to simulate by classical computers. As the circuits are too difficult to simulate, we simplified the circuits with depth 10 by reducing their depths to 5. The results are shown in Table VI, where all columns list the same information as that in Table III, except that memory usage information is additionally reported and the numbers of error and segmentation fault cases are all 0 and omitted. Similar to the experiments of Table III, we have 10 random circuits for each qubit size (in each row in Table VI), and the runtime was averaged over the cases that are simulated successfully. On the other hand, the memory usage was averaged over all 10 cases including TO and MO cases. The obtained results show that, DDSIM and our method suffer from MO and TO, respectively, when simulating $\#qubits \geq 42$. As can be observed, DDSIM took smaller average runtime compared to ours. However, by examining circuits with some specific $\#qubits$, we can observe that our method possibly simulates more cases than DDSIM. For example, when $\#qubits = 49$, our method simulates 9 cases, whereas DDSIM simulates only 4 cases. Overall, DDSIM simulates 74 out of the total 120 cases, whereas our method simulates 77 out of 120 cases. Furthermore, our method clearly outperforms DDSIM in terms of the memory usage. This challenging benchmark set motivates us for further investigation and improvement.

²There are other quantum algorithm circuits, such as QFT and Shor algorithms. However, they involve unitary operators not algebraically representable and are excluded from our experiments.

³The circuits were downloaded from <https://github.com/sboixo/GRCS> under the directory “inst/rectangular/cz_v2”.

TABLE III
RESULTS ON RANDOM CIRCUITS.

#Qubits	#Gates	DDSIM		Ours	
		Time(s)	TO/MO/err./seg.	Time(s)	TO/MO/err./seg.
40	120	8.67	0/0/0/0	0.82	0/0/0/0
80	240	502.29	2/6/0/0	14.62	0/0/0/0
120	360	failed	3/5/2/0	473.26	0/0/0/0
160	480	failed	0/2/8/0	617.38	2/0/0/0
200	600	failed	0/0/10/0	297.48	1/0/0/0
300	900	failed	0/0/10/0	647.98	5/0/0/0
400	1200	failed	0/0/0/10	2532.65	5/0/0/0
500	1500	failed	0/0/0/10	2485.64	9/0/0/0

TABLE IV
RESULTS ON REVLIB CIRCUITS.

Benchmark	#Qubits	Original				Modified			
		#Gates	Time(s)		#Gates	Time(s)			
			DDSIM	Ours		DDSIM	Ours		
_443	261	1251	0.31	0.17	1317	MO	166.55		
add64_184	193	256	0.05	0.05	385	0.14	0.09		
apex2_289	498	1746	0.59	0.46	1785	MO	4610.48		
callif_32_439	130	561	0.08	0.07	626	MO	3.68		
cps_292	923	2763	3.28	1.10	2787	MO	5059.14		
cpu_alu_16bit_400	405	6487	0.83	0.28	6526	MO	718.48		
cpu_control_unit_402	392	1351	0.24	0.09	1514	MO	1569.36		
cpu_register_32_405	328	597	0.35	0.07	890	0.53	0.35		
e64-bdd_295	195	387	0.11	0.06	452	3.08	3.03		
ex5p_296	206	647	0.14	0.08	655	1.43	11.54		
hwb9_304	170	699	0.13	0.07	708	5.84	12.53		
lu_326	299	571	0.19	0.25	637	MO	6.20		
nestedif2_32_445	263	854	0.24	0.23	920	MO	291.26		
pdc_307	619	2080	1.28	0.68	2096	MO	5856.65		
spla_315	489	1709	0.72	0.35	1725	MO	1925.49		
varops_32_447	224	1305	0.29	0.12	1401	MO	3271.49		

V. CONCLUSIONS

In this paper, we have presented a new quantum circuit simulator that outperforms the state-of-the-art in both scalability and accuracy. The algebraic representation, bit-slicing technique, and quantum gate formula pre-characterization together enable the success. For future work, we would like to investigate the supremacy benchmarks further and identify points for improvements.

ACKNOWLEDGMENT

This work was supported in part by the Ministry of Science and Technology of Taiwan under grant MOST 108-2218-E-002-073. The authors are grateful to Stefan Hillmich for answering questions about the DDSIM package.

REFERENCES

- [1] F. Arute *et al.*, “Quantum supremacy using a programmable superconducting processor,” *Nature*, vol. 574, pp. 505–510, 2019.
- [2] IBM Q. [Online]. Available: <https://www.research.ibm.com/ibm-q/>
- [3] H. Abraham *et al.*, “Qiskit: An open-source framework for quantum computing,” 2019.
- [4] S. Aaronson and D. Gottesman, “Improved simulation of stabilizer circuits,” *Physical Review A*, vol. 70, no. 5, Nov 2004.
- [5] A. S. Green, P. L. Lumsdaine, N. J. Ross, P. Selinger, and B. Valiron, “Quipper: A scalable quantum programming language,” in *ACM SIGPLAN Conference on Programming Language Design and Implementation, (PLDI)*, 2013, pp. 333–342.
- [6] D. Wecker and K. M. Svore, “Liqui|>: A software design architecture and domain-specific language for quantum computing,” 2014, arXiv: quant-ph/1402.4467.
- [7] N. Khammassi, I. Ashraf, X. Fu, C. G. Almudever, and K. Bertels, “QX: A high-performance quantum computer simulation platform,” in *Design, Automation and Test in Europe Conference and Exhibition (DATE)*, 2017, pp. 464–469.
- [8] E. Pednault *et al.*, “Breaking the 49-qubit barrier in the simulation of quantum circuits,” 2017, arXiv: quant-ph/1710.05867.

TABLE V
RESULTS ON QUANTUM ALGORITHM CIRCUITS.

#Qubits	Entanglement				BV		
	#Gates	Time(s)		#Gates	Time(s)		
		DDSIM	Ours		DDSIM	Ours	
80	80	0.01	0.02	239	0.02	0.06	
90	90	0.01	0.01	269	error	0.07	
100	100	0.01	0.01	299	error	0.07	
500	500	0.19	0.19	1499	seg. fault	4.48	
1000	1000	0.87	0.99	2999	seg. fault	116.80	
5000	5000	46.21	15.2	14999	seg. fault	186.93	
10000	10000	MO	66.95	29999	seg. fault	595.74	

TABLE VI
RESULTS ON GOOGLE SUPREMACY CIRCUITS.

#Qubits	#Gates	DDSIM			Ours		
		Time(s)	Mem(MB)	TO/MO	Time(s)	Mem(MB)	TO/MO
16	61	<0.01	86.99	0/0	0.14	62.91	0/0
20	79	0.01	86.99	0/0	1.09	76.13	0/0
25	99	0.01	87.00	0/0	4.38	98.66	0/0
30	120	0.01	87.00	0/0	4.19	100.30	0/0
36	144	0.58	90.87	0/0	25.86	111.12	0/0
42	169	0.16	871.63	0/4	938.06	136.50	1/0
49	202	4.50	1274.99	0/6	2095.56	248.86	1/0
56	225	93.24	944.89	0/3	1478.19	249.74	5/0
64	254	10.66	1286.31	0/6	3339.24	335.49	6/0
72	290	613.29	1791.28	0/8	failed	373.52	10/0
81	328	2.22	1795.43	1/8	failed	278.66	10/0
90	365	failed	1745.23	3/7	failed	347.84	10/0

- [9] D. S. Steiger, T. Hner, and M. Troyer, “ProjectQ: An open source software framework for quantum computing,” *Quantum*, vol. 2, p. 49, Jan 2018.
- [10] G. F. Viamontes, I. L. Markov, and J. P. Hayes, *Quantum Circuit Simulation*. Springer Publishing Company, Incorporated, 2009.
- [11] V. Samoladas, “Improved BDD algorithms for the simulation of quantum circuits,” in *European Symposium on Algorithms (ESA)*, 2008, pp. 720–731.
- [12] A. Zulehner and R. Wille, “Advanced simulation of quantum computations,” *Trans. on CAD of Integrated Circuits and Systems*, vol. 38, no. 5, pp. 848–859, 2019.
- [13] A. Zulehner, S. Hillmich, and R. Wille, “How to efficiently handle complex values? Implementing decision diagrams for quantum computing,” in *International Conference on Computer-Aided Design (ICCAD)*, 2019, pp. 1–7.
- [14] P. Niemann, R. Wille, D. M. Miller, M. A. Thornton, and R. Drechsler, “QMDDs: Efficient quantum function representation and manipulation,” *IEEE Transactions on Computer-Aided Design of Integrated Circuits and Systems*, vol. 35, no. 1, pp. 86–99, 2016.
- [15] A. Zulehner, P. Niemann, R. Drechsler, and R. Wille, “Accuracy and compactness in decision diagrams for quantum computation,” in *Design, Automation and Test in Europe Conference and Exhibition (DATE)*, 2019, pp. 280–283.
- [16] P. O. Boykin, T. Mor, M. Pulver, V. Roychowdhury, and F. Vatan, “A new universal and fault-tolerant quantum basis,” *Inf. Process. Lett.*, vol. 75, no. 3, p. 101107, 2000.
- [17] D. Aharonov, “A simple proof that Toffoli and Hadamard are quantum universal,” 2003, arXiv: quant-ph/0301040.
- [18] J.-H. R. Jiang, J.-Y. Jou, and J.-D. Huang, “Compatible class encoding in hyper-function decomposition for FPGA synthesis,” in *Design and Automation Conference (DAC)*, 1998, pp. 712–717.
- [19] R. Brayton and A. Mishchenko, “ABC: An Academic Industrial-Strength Verification Tool,” in *Proceedings of International Conference on Computer Aided Verification (CAV)*, 2010, pp. 24–40.
- [20] F. Somenzi, “CUDD: CU decision diagram package (release 2.4.2),” *University of Colorado at Boulder*, 2005.
- [21] S. Panda, F. Somenzi, and B. F. Plessier, “Symmetry detection and dynamic variable ordering of decision diagrams,” in *International Conference on Computer-Aided Design (ICCAD)*, 1994, p. 628631.
- [22] L. Fousse, G. Hanrot, V. Lefèvre, P. Pélissier, and P. Zimmermann, “MPFR: A multiple-precision binary floating-point library with correct rounding,” *ACM Trans. Math. Softw.*, vol. 33, no. 2, p. 13es, Jun. 2007.
- [23] R. Wille, D. Große, L. Teuber, G. W. Dueck, and R. Drechsler, “RevLib: An online resource for reversible functions and reversible

circuits,” in *Int’l Symp. on Multi-Valued Logic*, 2008, pp. 220–225,
<http://www.revlb.org>.

- [24] E. Bernstein and U. Vazirani, “Quantum complexity theory,” *SIAM J. Comput.*, vol. 26, no. 5, p. 14111473, Oct. 1997.
- [25] S. Boixo *et al.*, “Characterizing quantum supremacy in near-term devices,” *Nature Physics*, vol. 14, no. 6, p. 595600, Apr 2018.
- [26] S. Aaronson and D. Gottesman, “CHP: CNOT-Hadamard-Phase.” [Online]. Available: <https://www.scottaaronson.com/chp/>